

Contents lists available at ScienceDirect

Spectrochimica Acta Part B

journal homepage: www.elsevier.com/locate/sab



Multivariate classification of edible salts: Simultaneous Laser-Induced Breakdown Spectroscopy and Laser-Ablation Inductively Coupled Plasma Mass Spectrometry Analysis



Yonghoon Lee ^{a,*}, Sang-Ho Nam ^a, Kyung-Sik Ham ^b, Jhanis Gonzalez ^{c,d}, Dayana Oropeza ^{c,d}, Derrick Quarles Jr. ^{c,d}, Jonghyun Yoo ^d, Richard E. Russo ^{c,d}

- ^a Department of Chemistry, Mokpo National University, Jeonnam 534-729, Republic of Korea
- ^b Department of Food Engineering, Mokpo National University, Jeonnam 534-729, Republic of Korea
- ^c Environmental Energy Technology Division, Lawrence Berkeley National Laboratory, Berkeley, CA 94720, United States
- ^d Applied Spectra, Inc., 46665 Fremont Boulevard, Fremont, CA 94538, United States

ARTICLE INFO

Article history: Received 17 August 2015 Revised 12 November 2015 Accepted 27 February 2016 Available online 03 March 2016

Key words:
Laser-Induced Breakdown Spectroscopy
Laser-Ablation Inductively Coupled Plasma
Mass Spectrometry
Edible salts
Classification
Discrimination power

ABSTRACT

Laser-Induced Breakdown Spectroscopy (LIBS) and Laser-Ablation Inductively Coupled Plasma Mass Spectrometry (LA-ICP-MS), both based on laser ablation sampling, can be employed simultaneously to obtain different chemical fingerprints from a sample. We demonstrated that this analysis approach can provide complementary information for improved classification of edible salts. LIBS could detect several of the minor metallic elements along with Na and Cl, while LA-ICP-MS spectra were used to measure non-metallic and trace heavy metal elements. Principal component analysis using LIBS and LA-ICP-MS spectra showed that their major spectral variations classified the sample salts in different ways. Three classification models were developed by using partial least squares-discriminant analysis based on the LIBS, LA-ICP-MS, and their fused data. From the cross-validation performances and confusion matrices of these models, the minor metallic elements (Mg, Ca, and K) detected by LIBS and the non-metallic (I) and trace heavy metal (Ba, W, and Pb) elements detected by LA-ICP-MS provided complementary chemical information to distinguish particular salt samples.

© 2016 Elsevier B.V. All rights reserved.

1. Introduction

Salt, a natural ionic-compound mixture with a NaCl matrix, is used ubiquitously as a food additive. According to recent studies, an average person consumes salt ranging from a few to 10 g per day [1,2]. Salt intake is accompanied by absorption of Na, which is known to be related to human diseases such as hypertension and diabetes [3–6]. Salts are generally produced by evaporating seawater (sea salt) on saltpans or extracted from underground areas (rock salt) where the sea had been previously [7]. Some of these unrefined salts contain high-level of mineral elements such as K, Mg, and Ca, which are dissolved in the seawater. These elements are considered as alternative nutrition sources and mitigate the high Na intake; their potential health benefits have been suggested [8–11].

Although the main component of unrefined salts is NaCl, the chemical composition exhibits a wide variety of minor elements. In the case of sea salts, the chemical composition is not simply that of

seawater. The concentrations of the minor metallic mineral elements, K, Mg, and Ca, originally dissolved in seawater, show large variation with the density of brine water extracted from the reservoir into the evaporation and crystallization areas of the saltpans [12,13]. Also, when the saltpan is open to the surrounding environment, the dried salts tend to contain relatively high concentration of soil particles [14,15], leading to higher concentrations of rockforming elements (Al, Ti, Si, and Fe). For rock salts, their chemical composition is originally based on that of the ancient seawater. However, inclusion of rock particles, interaction with underground fresh water, and chemical reactions facilitated thermally underground can change the chemical composition of rock salts. The chemical composition in unrefined salts can be utilized as reliable fingerprints for classifying them according to their geographical origin or discriminating a certain salt from others.

Today, salt markets in many countries have been globalized and premium unrefined salts are attracting more interests. Therefore, effective chemical methodologies are necessary to identify the salt products circulated in these markets. So far, a few chemical analysis techniques and effective indicators have been suggested for this purpose. Herrador et al. reported that K, Mg, and Sr can be used as dependable indicators for edible salts marketed in Spain by using inductively coupled

^{*} Corresponding author. E-mail address: yhlee@mokpo.ac.kr (Y. Lee).

plasma-atomic emission spectrometry (ICP-AES) [16]. Silva et al. identified ~40 volatile organic compounds in sea salts by gas chromatography-mass spectrometry and suggested that those organic compounds serve as chemical biomarkers of sea salts thus providing information about the geographical origin and saltpan environment [17]. Galvis-Sánchez et al. applied Fourier-transform near-infrared spectroscopy for discriminating sea salts according to their quality and geographical origin [12].

Laser-Induced Breakdown Spectroscopy (LIBS) and Laser-Ablation Inductively Coupled Plasma Mass Spectrometry (LA-ICP-MS) are elemental analysis techniques based on laser ablation [18-19] and have rapidly expanded their applications in various fields [20-22]. Both LIBS and LA-ICP-MS share the strength of spatially-resolved multielemental analysis with little to no sample preparation; laser ablation is the underlying sampling process. However, their analytical characteristics and figures of merit are different since the nature of their signals is different; the intensity and wavelength of photons versus the mass-tocharge ratio (m/z) of particles for LIBS and LA-ICP-MS, respectively. In general, LIBS utilizes simpler instrumentation and for many cases the analysis can be performed under ambient conditions. Typical limits of detection of metallic elements reported for LIBS are parts-permillion (ppm) to wt.% levels. On the other hand, LA-ICP-MS can reach lower concentrations on the order of sub-ppm levels [23–24]. Although recently it has been found that isotopic information can be obtained from the molecular emission from laser-induced plasmas [25], conventional ICP-MS and LA-ICP-MS have been generally used for the accurate isotopic analysis [26]. Therefore, the combination of LIBS and LA-ICP-MS can be used to obtain chemical information over a wider concentration range. There are a few recent studies where simultaneous LIBS and LA-ICP-MS made synergistic improvements in quantitative and qualitative analyses [27–31]. For example, Dong et al. showed how this combination more accurately predicted the major, minor and trace elemental concentrations from coal samples [27].

We previously demonstrated the feasibility of rapid classification of edible salts by using multivariate data analysis of LIBS emission spectra [14,15,32]. The edible sea salts, recognized for rich mineral elements, typically contain K, Mg, and Ca with concentrations of several thousand ppm to a few % [15,32,33]. K, Ca, and Mg play important roles in classification of salts, but these elements are not well detected by the ICP-MS due to overlap of abundant molecular species in ICP plasmas [36,37]. Other elements (Li, Sr, Al, Ti, Si, and Fe) can be detected by LIBS if their concentrations in these salts are at the ppm level or higher [14]. In addition, there are other trace elements in edible salts that could provide unique discrimination power for particular salts, but they are not detected by LIBS due to their low concentrations [34,35]. The chemical composition and quantity of these trace elements could reflect the effects of natural environments or contamination around the saltpans. The combination of LIBS and LA-ICP-MS provides chemical analysis covering light metals at several hundred ppm to a few % levels, non-metals, and trace heavy metals at subppm levels.

In this work, we demonstrated simultaneous LIBS and LA-ICP-MS analysis for improved classification of edible salts. LIBS was optimized for the detection of the light elements including K, Mg, and Ca. LA-ICP-MS analysis emphasized elements with $m/z \ge 90$, including non-metal and trace heavy metal elements. Our results demonstrate that LIBS and LA-ICP-MS spectra provide complementary discrimination power for the classification of these edible salts. Herein, the term "discrimination power", means the ability of variables of LIBS or LA-ICP-MS spectra to discriminate a certain salt sample from the others [38]. The classification model based on LIBS spectra of minor metallic elements showed high performance, whereas the chemical information on non-metallic and trace heavy metal elements obtained from LA-ICP-MS spectra added unique discrimination power to the classification model based on the fused data.

2. Experimental

2.1. Salt samples

Fourteen salt samples were collected from ten countries. The geographical origin and type of sample salts are listed in Table 1. The salts from Mongolia, Poland, India, and Pakistan are rock salts and the others are sea salts. Each salt sample was milled and homogenized into a fine powder using a ball mill (8000 M Mixer/Mill®, SPEX Sample Prep). Five grams of each salt was put in an agate vial with an agate ball and then rotated at 1450 rpm for 5 min. A half gram of the milled salt powder was pelletized into a 13-mm diameter disk by an automated press (3630 X-PRESS®, SPEX Sample Prep) under 7 ton pressure for 10 min.

2.2. LIBS and LA-ICP-MS measurements

Simultaneous LIBS and LA-ICP-MS measurements were performed using a commercial instrument (J200 Tandem LA-LIBS Instrument, Applied Spectra, Inc.). A Q-switched Nd:YAG laser beam was focused on the surface of salt samples by an objective lens ($5 \times$ magnification, 35 mm working distance). The wavelength, pulse duration, pulse energy, repetition rate, and spot size on the sample surface were 266 nm, 10 ns, 20 mJ/pulse, 10 Hz, and 150 µm in diameter, respectively. These conditions provided good S/N for both LIBS and LA-ICP-MS measurements. Helium was used as the chamber gas. For each salt pellet, an area of 3 mm² (1.5 mm \times 2 mm) on the surface was sampled by a raster scan composed of 2955 laser shots. During the analysis, the sample stage was translated at the rate of 0.1 mm/s. For the LIBS measurements, the optical emission from the laser-induced plasma was collected by two lenses through the top quartz window and sent to a 6-channel charge-coupled device (CCD) spectrometer with ~0.1 nm spectral resolution and wavelength coverage between 190 and 1040 nm. The CCD detection gate with 1.05 ms width was delayed from the laser pulse by 1 µs to minimize continuum background emission and spectral line broadening. 123 single-shot spectra were accumulated for each spectrum to be analyzed.

A quadrupole based mass spectrometer (Plasma Quant MS Elite, Analytik Jena) was used for the ICP-MS measurements. The He carrier gas flow rate was set to 0.3 L/min. The forward power for plasma generation was set to 1400 W with 18.0 L/min Ar gas, auxiliary flow rate of 1.8 L/min and sheath gas flow rates of 0.8 L/min. The mass spectra for *m/z* of 6 to 239 were recorded. The *m/z* values (8, 12, 14–26, 28, 30, 32, 35–44, 48, 56, 80, 210–219, and 221–225) were skipped to avoid saturated signals from the background gas (C, O, N, Ar, etc.), the major elements of salts (Na, Cl, Mg, Ca, and K), and molecular ions. Data acquisition for LA-ICP-MS and LIBS were synchronized. A single scan of the mass spectrum required 12.3 s. For each salt sample, 18–23 pairs of accumulated LIBS and LA-ICP-MS spectra were collected.

Additional LIBS experiments were performed in open air. The experimental conditions and parameters were the same as those used for the LIBS part of the simultaneous LIBS and LA-ICP-MS experiments above, except for the ambient gas. The LIBS spectra (in He and air) were analyzed to check if non-metallic and trace heavy metal elements detected by LA-ICP-MS are also detected in the LIBS spectra recorded in air.

3. Results and discussion

3.1. LIBS and LA-ICP-MS spectra

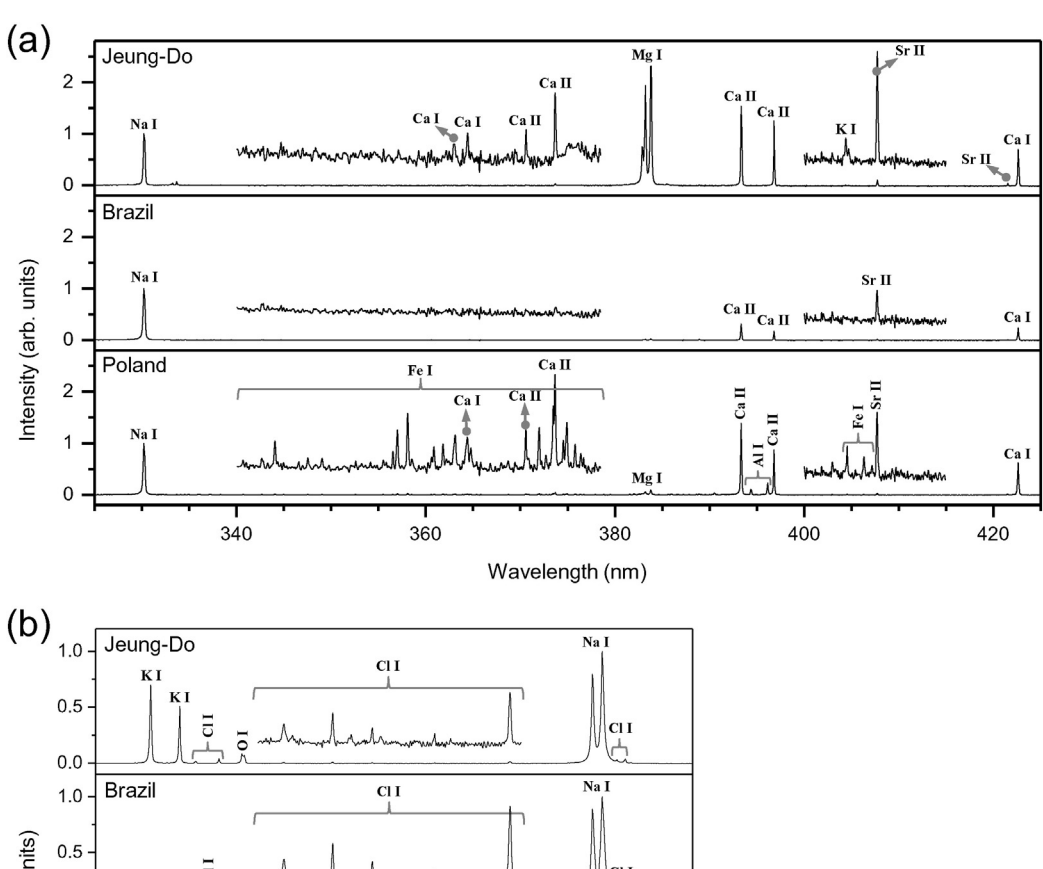
Fig. 1 shows the averaged LIBS spectra of the salt samples from Jeung-Do, Brazil, and Poland in wavelength regions, 325–425 nm (a) and 760–830 nm (b), with assignments of the observed emission lines based on the NIST Atomic Spectra Database [39]. Na I, Ca I and II, Mg I, Sr II, Fe I, and Al I lines are observed in the ultraviolet–visible region (Fig. 1a). K I, Cl I, O I, and Na I lines are observed in the near-infrared region (Fig. 1b). For the multivariate analysis, we selected

Table 1Geographical origin and types of the sample salts and the elements identified in LIBS and LA-ICP-MS spectra. Na, Cl, and He, identified in all samples, were not included.

Sample no.	Geographical origin	Туре	Elements identified in LIBS spectra	Elements identified in LA-ICP-MS spectra
1	Laizhou, China	Sea salt	Si, Al, Mg, Ca, K, Sr, Li, O, H	Zr, Nb, Mo, Ag, Cd, Sn, I, Cs, Ba, La, Ce, W, Pb
2	Okinawa, Japan	Sea salt	Mg, Ca, K, Sr, Li, S, O, H	Mo, Sn, I, Cs, Ba
3	Hokkaido, Japan	Sea salt	Mg, Ca, K, Li, S, O, H	Mo, Sn, I, Cs, Ba
4	Kochi, Japan	Sea salt	Mg, Ca, K, Sr, Li, S, O, H	Mo, Ag, Cd, Sn, I, Cs, Ba, La, Ce, W, Pb
5	Jeung-Do, South Korea	Sea salt	Mg, Ca, K, Sr, Li, S, O, H	Zr, Nb, Mo, Ag, Cd, Sn, I, Cs, Ba, La, Ce, Pb
6	Haenam, South Korea	Sea salt	Si, Al, Mg, Ca, K, Sr, Li, S, O, H	Zr, Nb, Mo, Ag, Sn, I, Cs, Ba, La, Ce, W, Pb
7	Younggwang, South Korea	Sea salt	Si, Al, Mg, Ca, K, Sr, Li, S, O, H	Zr, Nb, Mo, Ag, Sn, I, Cs, Ba, La, Ce, W, Pb
8	Guerande, France	Sea salt	Si, Al, Mg, Ca, K, Sr, Li, S, O, H	Zr, Nb, Mo, Cd, Sn, I, Cs, Ba, La, Ce, Pb
9	Brazil	Sea salt	Mg, Ca, K, Sr, O, H	Sn, I, Cs, Ba
10	Chile	Sea salt	Mg, Ca, K, Sr, O, H	Sn, I, Cs, Ba
11	Mongolia	Rock salt	Ca, K, Li, O, H	Zr, Mo, Sn I, Ba, Pb
12	Poland	Rock salt	Fe, Si, Al, Mg, Ti, Ca, K, Sr, Li, S, O, H	Zr, Nb, Mo, Sn, I, Cs, Ba, La, Ce, Pb
13	Himalaya, India	Rock salt	Fe, Si, Al, Ti, Ca, K, Sr, Li, S, O, H	Zr, Nb, Mo, Sn, I, Cs, Ba, La, Ce, W, Pb
14	Himalaya, Pakistan	Rock salt	Si, Al, Mg, Ca, K, Sr, Li, S, O, H	Zr, Nb, Sn, I, Cs, Ba, La, Ce, Pb

wavelength regions, 362–410 nm and 765–771 nm, instead of the full LIBS spectra between 190 and 1040 nm. This choice is based on the line-intensity correlation analysis for the LIBS spectra of sea salts [14] and the consideration of differences of chemical composition between sea and rock salts. The partial least squares-discriminant analysis

(PLS-DA) model developed using the LIBS spectra in the selected wavelength regions including Mg I, Ca I and II, Sr II, Al I, Fe I, and K I lines shows similar classification performance to that using the full LIBS spectral range. We compared their cross-validation correctness (Fig. 6a) and confusion matrices (Fig. S1 in the Supplementary content).



1.0 - Brazil CII Na I

(\$\frac{1}{10} = \frac{1}{10} = \frac{1}{10

Fig. 1. Averaged LIBS spectra of the salt samples from Jeung-Do, Brazil, and Poland in two different wavelength regions: 325–425 nm (a) and 760–830 nm (b) with assignments of the observed emission lines.

This similarity indicates that these emission lines can represent most of the features of the full LIBS spectra that are correlated to the origin of the sample salts. This wavelength selection significantly reduced the number of data points to be processed and thus led to efficient data analysis. In the following, the chemical background of this wavelength selection is discussed.

The salts from Jeung-Do and Brazil can be regarded as representatives for different types of sea salts. The salt from Jeung-Do is one of the mineral-rich sea salts with high concentrations of Mg, Ca, and K up to a few %. Thus, in the LIBS spectrum of the Jeung-Do sample, strong Mg I, Ca I and II, and K I lines were observed. On the other hand, there are some sea salts with very low concentrations of Mg, Ca, and K. The sample from Brazil represents these mineral-deficient sea salts. In the LIBS spectra of the sea salt from Brazil, the Mg I, Ca I and II, and K I lines are very weak compared to those observed from the Jeung-Do salt sample. Thus, these samples represent the two extreme cases; mineral-rich and mineral-deficient sea salts. Previously, Mg and K concentrations in sea salts were found to have strong positive correlation with a coefficient of 0.917 (see Figure 6c in Ref. 14). This can be attributed to the fact that both Mg and K in sea salts come from the same source (dissolved ions, K⁺ and Mg²⁺, in seawater). The strong positive correlation between Mg and K concentrations in sea salts makes their discrimination power for sea salts not independent. Therefore, most of the discrimination power from the LIBS spectra could be utilized by considering a few emission lines of Mg, and Ca or K, and Ca along with the Al line discriminating particular sea salts containing relatively large amount of soil particles [14,15]. The Al concentration is correlated to that of the other rock-forming elements, Ti, Si, and Fe [14].

The LIBS spectrum of the rock salt from Poland (Fig. 1) is used to explain the difference between sea salt and rock salt samples. The variation of LIBS spectral features within rock salt samples is not as significant as that for sea salts. The LIBS spectra of the rock salt from Poland exhibits very weak Mg I lines around 383 nm although the K I lines at 766.5 and 769.9 nm exhibit strong intensities. Although the chemical composition of rock salts is originally based on that of ancient seawater, the Mg concentration in rock salts is frequently very low due to the high solubility of Mg-containing ionic compound, probably MgSO₄, from the original seawater that can be easily removed by underground freshwater. Thus, the correlation between Mg and K can be weak in rock salts and their discrimination power would be less dependent on each other than that for sea salts. Another characteristic of the LIBS spectra of rock salts is the strong emission lines of the rockforming elements (Al, Si, Ti and Fe), which might have been incorporated in the rock salts during the mining process. In the LIBS spectrum of the rock salt from Poland, both Fe I and Al I lines show relatively strong intensities in comparison with those of the other samples.

In the other wavelength regions, most of the prominent emission lines are from Na, Cl, Mg, and Ca, with weak emission lines from Sr, Al, Li, Ti, Fe, C, and Si. The detailed assignments of the emission lines in the full wavelength region can be found in Figures 1 and 2 of Ref. 14. The spectral intensities for the selected wavelength regions were normalized. The Na I line intensities at 330.2 and 819.5 nm were employed for spectral intensity normalization as reference signals in the shorter and longer wavelength regions, respectively, since they are weak emission lines of major matrix elements located closely to the analyte signals [40].

Fig. 2 shows LA-ICP-MS data for the salts from Haenam, Hokkaido, Chile, Brazil, India, and Poland. The mass peaks corresponding to Zr, Mo, Nb, Sn, I, Cs, Ba, La, Ce (and other lanthanides), W, and Pb isotopes were assigned. There are additional mass peaks at m/z=104, 129, 130, 131, 132, 134, and 136. Considering the intensities, the mass peak at m/z=104 are not assignable to any stable isotopes and tentatively attributed to 88 Sr 16 O formed in the ICP. The other masses are assigned to the isotopes of Xe added in the Ar ICP plasma gas as impurity. The LA-ICP-MS spectra shown in Fig. 2 indicate that the salt samples have quite different chemical compositions of heavy elements. The elements,

Ba, W, Pb, I, Sn, Mo, Zr, Nb, La, Ce, etc. provide significant power for differentiating individual salt sample. The complementarity between some of these elements and those detected by LIBS is discussed in Section 3.3. For normalization of the LA-ICP-MS spectra, we could not use the weak isotope peaks from major matrix elements Na and Cl. Therefore, the total intensity of each LA-ICP-MS spectrum (m/z=6-239) was used as a reference signal for intensity normalization.

3.2. LIBS LA-ICP-MS data fusion

We performed principal component analyses (PCAs) for the LIBS, LA-ICP-MS, and their fused spectra using the Unscrambler X program (CAMO Software). The normalized spectra were mean-centered prior to the PCA. Fig. 3 shows loadings for PC1 and PC2 (a) and the corresponding score plot (b) obtained from PCA of the LIBS spectra. In the PC loading plots, the variables corresponding to Mg I, Ca II and I, K I, and Al I lines are indicated. From the loading plot of PC1, it was found that the chemical composition of our salt samples shows large variations in concentrations of Mg, Ca, and K and their variations are mainly positively correlated. Also, the loadings of PC2 indicate that the negative correlation between the concentrations of Mg and Ca are necessary to explain the second most significant variation of chemical composition for our samples. According to the score of PC1, the sample salts can be roughly categorized into three groups (A, B and C in Fig. 3b), Although this grouping is not from any statistical analysis, their separation along the PC1 axis is clear. The salt samples from Jeung-Do, Okinawa, and Kochi consist of the sea salt group with relatively high concentrations of Mg, Ca, and K (group A). The salts from Guerande, Younggwang, Haenam, and Hokkaido form the other sea salt group (group B). The lower PC1 scores of the salts in group B (around 0-1) than those of group A (1.5–4) indicates that the concentrations of Mg, Ca, and K in the salts in group B would be less than those in the salts in group A. All of the salts in groups A and B are sea salts. However, group C includes both sea and rock salts. The PC1 and PC2 scores of the samples in group C show clear positive correlation as indicated by the arrow in Fig. 3b. This positive correlation between PC1 and PC2 scores indicates that they have very small amount of Mg in common (opposite signs of the PC1 and PC2 loadings corresponding to the Mg I lines in Fig. 3a). However, the concentrations of Ca and K show variations to some extent, but their small PC 1 scores indicate that the concentrations are less than those of Ca and K in the salts in groups A and B. In group A, PC2 scores of the Jeung-Do sample are separated from those of the other two samples from Okinawa and Kochi although these three samples have similar PC1 scores. This is due to the smaller intensity ratio of Ca II to Mg I lines observed in the LIBS spectra of the Jeung-Do sample than those of the others (Fig. S2 in the Supplementary content).

Fig. 4 shows the loadings of PC1 and PC2 (a) and the corresponding score plot (b) obtained from the PCA of the LA-ICP-MS spectra. The variables corresponding to Zr, Mo, Sn, I, Ba, W, and Pb are indicated in the PC loading plots. These elements in the salt samples were undetectable by LIBS. The PC score plot based on the LA-ICP-MS spectra (Fig. 4b) shows a significantly different clustering pattern from that based on the LIBS spectra (Fig. 3b). These results show that the two chemical fingerprints recorded by LIBS and LA-ICP-MS are independent in terms of the main spectral variations (PC1 and PC2). The sea salts from Chile and Laizhou form two separate extreme clusters. For the salt from Chile, its high scores for PC1 and PC2 indicate that it contains relatively large amount of I and that the concentrations of W and Pb are very low. For the salts from Laizhou, the most negative PC1 and positive PC2 scores indicate that it contains relatively high concentrations of W and Pb and low concentration of I.

A simple data fusion method was used to combine the independent discrimination powers of the LIBS and LA-ICP-MS spectra. Each LA-ICP-MS spectrum was stitched at the end of the simultaneously recorded LIBS spectrum after being multiplied by a weighting factor (WF), varying the WF from 1 to 5000. Fig. 5 shows the PC score plots obtained

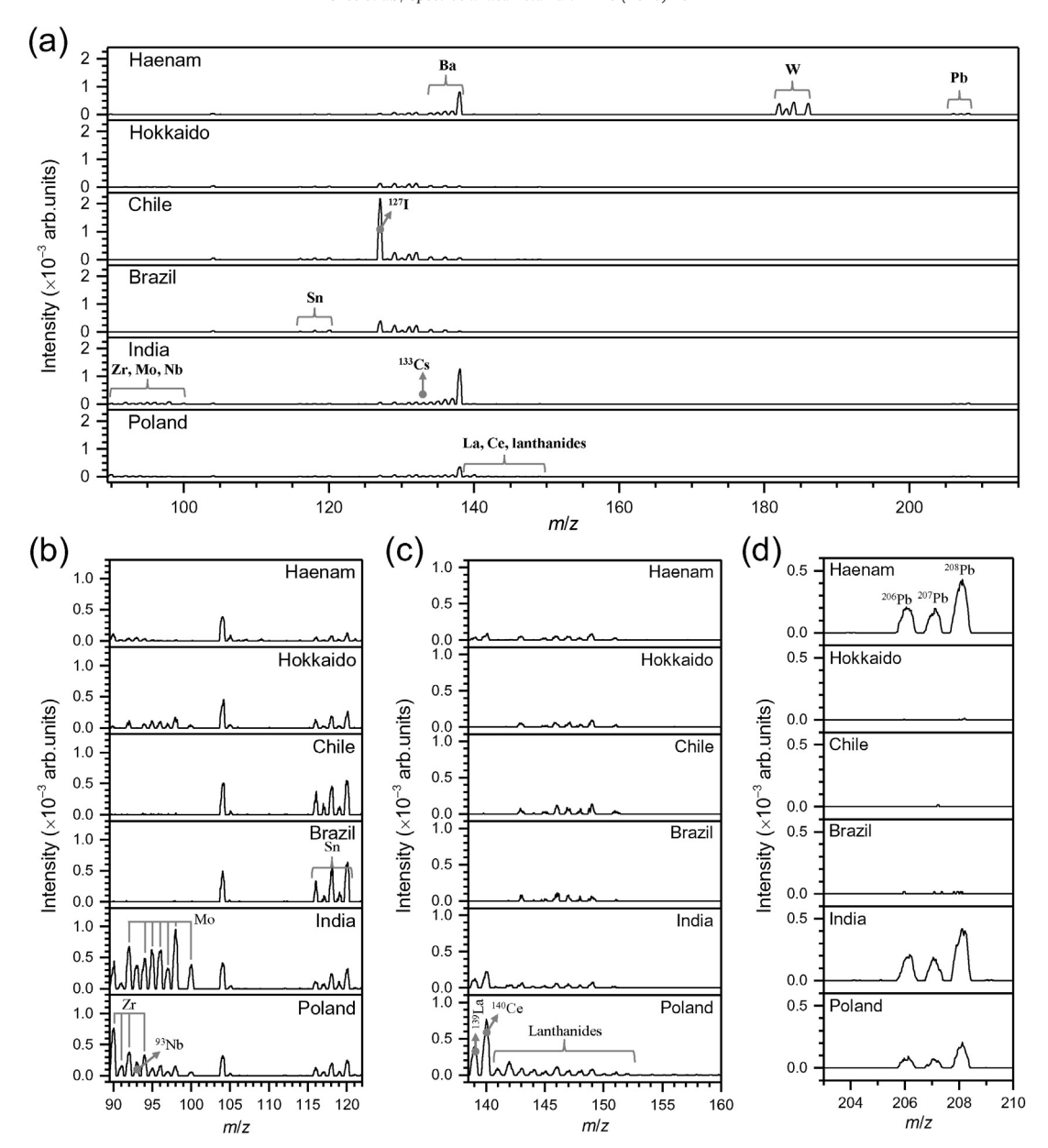


Fig. 2. MS spectra of the salts from Haenam, Hokkaido, Chile, Brazil, India, and Poland recorded by the LA-ICP-MS in the range of m/z = 90-215 (a) and the expanded LA-ICP-MS spectra in the ranges of m/z = 89.5-122 (b), 138.5-160 (c), and 203-210 (d).

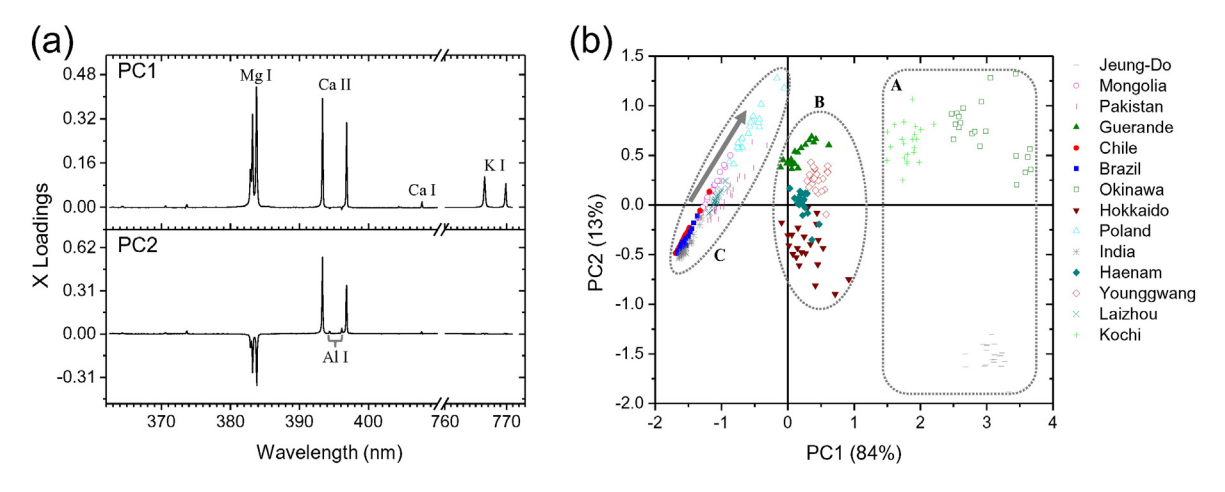


Fig. 3. Loadings of PC1 and PC2 (a) and the corresponding score plot (b) obtained from PCA of the LIBS spectra. The arrow in the circle of group C in b indicates the positive correlation between the PC1 and PC2 scores of the samples in group C.

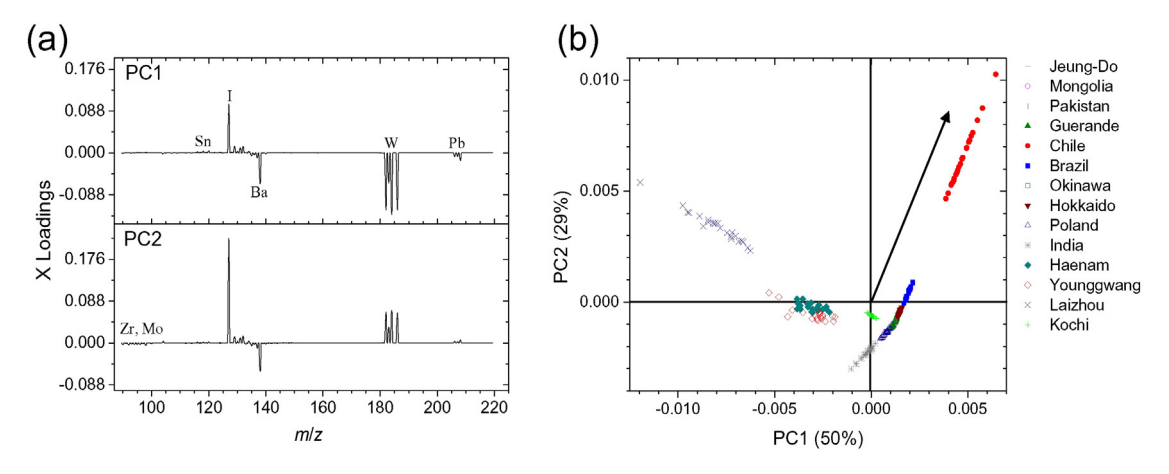


Fig. 4. Loadings of PC1 and PC2 (a) and the corresponding score plot (b) obtained from the PCA of the LA-ICP-MS spectra.

from the LIBS spectra (a), LA-ICP-MS spectra (h), and their fused data (b-g). The PC score plots obtained from the fused data with the different WF values for the LA-ICP-MS spectra, 1, 100, 250, 500, 750, and 5000 are

shown in Figs. 5b–g, respectively. When the WFs are relatively small (1 and 100), the fused-data-based PC scores show similar clustering patterns to that from the LIBS spectra. With relatively large WFs (750 and

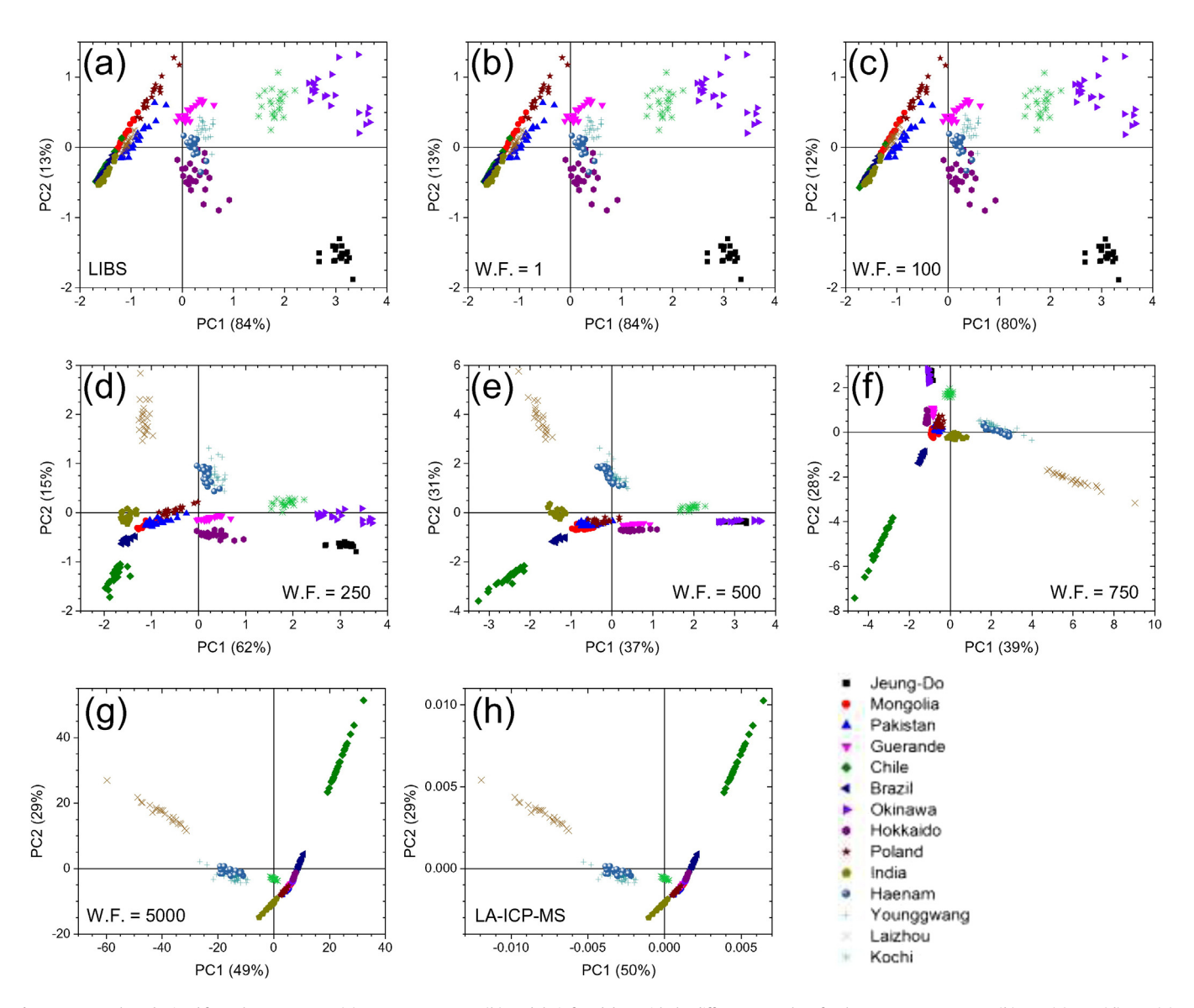


Fig. 5. PC score plots obtained from the LIBS spectra (a), LA-ICP-MS spectra (h), and their fused data with the different WF values for the LA-ICP-MS spectra, 1 (b), 100 (c), 250 (d), 500 (e), 750 (f), and 5000 (g).

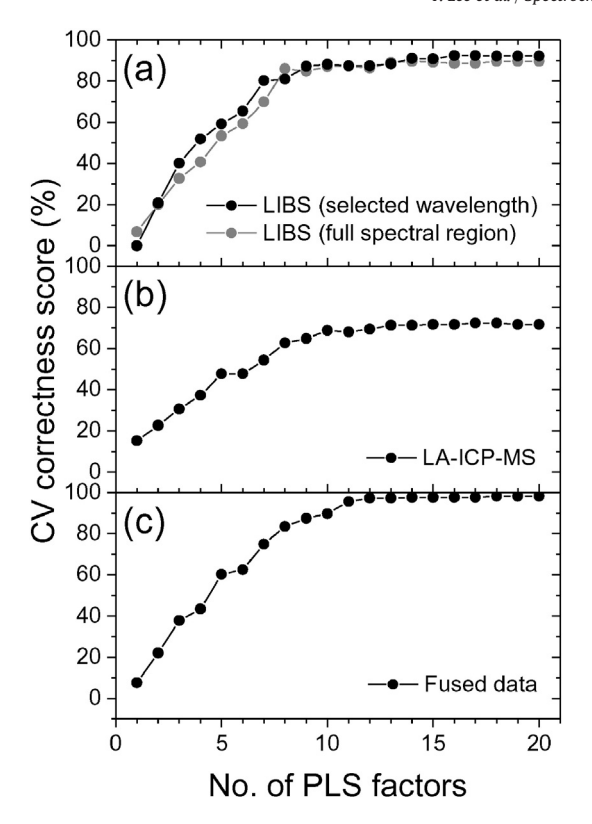


Fig. 6. CV correctness of the three PLS-DA models based on LIBS (a), LA-ICP-MS (b), and their fused data (c). In a, the CV correctness scores from the LIBS-based model using the spectra in full wavelength region to compare with those obtained using the LIBS spectra in the selected wavelength regions.

5000), the corresponding PC score plots are similar to that from the LA-ICP-MS spectra. Note that only the ranks of PC1 and PC2 were changed for the PC score plot in Fig. 5f (WF = 750) and the clustering pattern is similar to that in Fig. 5g. Therefore, effective data fusion would be obtained with the intermediate WFs = 250 and 500. The WF = 250 shows the best separation among the individual clusters; the nine salts of the fourteen total samples form their own clusters well separated from the others.

Herein, we investigated how LIBS, LA-ICP-MS, and their fused data distinguish the sample salts in terms of main spectral variations, PC1 and PC2. According to the later PCs such as PC3 and PC4 extracted from the LIBS, LA-ICP-MS and their fused data, the relevant PC scores form clusters. The loadings of PC3 and PC4 along with those of PC1 and PC2 and the PC1-PC3 and PC1-PC4 score plots can be found in the Supplementary content (Figs. S3-S5).

3.3. Classification models

We tested three PLS-DA classification models based on the LIBS, LA-ICP-MS, and their fused data with WF = 250 for the 14 salt samples listed in Table 1. A LIBS Graphical Development Tool (LIBS GDT, New Folder Consulting) was used for the PLS-DA analysis. The model performances were validated by using a cross-validation (CV) method with a leave-one-out (LOO) algorithm [41]. In the validation process, we made as many sub-models as there are spectra, each time leaving out just one of the objects and only using this for testing (classifying the sample identity of the spectrum kept from the data set for modeling). The correctness scores for testing were obtained for the models with different numbers of PLS factors from 1 to 20. In Fig. 6, the CV correctness scores are plotted with respect to the numbers of PLS factors included in the models based on the LIBS, LA-ICP-MS and their fused data. In Fig. 6a, the CV correctness scores

from the LIBS-based model using the spectra in the full wavelength region are compared with those obtained using the LIBS spectra in the selected wavelength regions. From this comparison, inclusion of all data points in the full wavelength region is found to be ineffective. Furthermore, the models using the LIBS spectra in the full

(a) LIBS model

	Guerande Haenam	0	0	100	48	19	0	0	0	0	0	0	0	0	33
	Hokkaido	0	0	0	0	100	0	- 0	-0	0	0	0	0	0	0
_	India	0	0	0	0	0	100	0	.0	0	0	0	0	0	0
Truth	Jeung-Do	0	0	0	0	0	0	100	0	0	0	0	0	0	0
	Kochi	0	0	0	0	0	0	0	100	0	0	0	0	0	0
	Laizhou	0	0	0	0	. 0	0	0	0	100	0	0	0	0	0
	Mongolia	0	.0	0	-0	0	0	0	-0	0	100	0	-0	0	0
	Okinawa	. 0	0	0	0	0	0	0	0	0	0	95	0	0	5
	Pakistan	0	0	5	0	0	0	0	0	0	9	0	86	0	0
	Poland	0	0	0	0	0	0	0	0	0	0	0	0	100	0
	Younggwang	0	0	0	0	- 5	0	_0	_ 0	0	0	0	0	0	95
		Brazil	Chile	Guerande	Haenam	Hokkaido	india	Jeung-Do	Kochí	Laizhou	Mangolia	Okinawa	Pakistan	Poland	3uew38uno,

Response

(b) LA-ICP-MS model

	Brazil	.9	0	0	0	0	0	0	0	0	91	0	0	0	0
	Chile	0	100	0	0	0	0	0	.0	0	0	0	0	0	0
	Guerande	0	0	22	0	0	0	0	0	0	0	67	-0	11	0
	Haenam	0	0	0	71	0	0	0	0	0	0	.0	0	O	29
	Hokkaido	. 5	0	0	-0	73	0	0	0	0	5	18	Đ	0	0
	India	0	0	0	.0	. 0	100	0	0	0	0	0	.0	0	0
Truth	Jeung-Do	0	Ó	0	0	. 5	. 0	0	0	0	0	95	0	0	0
르	Kochi	0	0	0	0	0	0	0	100	.0	0	0	Ø	Ó	0
	Laizhou	0	0	0	0	0	0	0	0	100	0	. 0	0	0 0	0
	Mongolia	. 5	0	0	- 0	0	0	- 0	0	0	95	0	D	0	0
	Okinawa	0	0	0	0	0	0	0	. 0	0	0	100	0	0	0
	Pakistan	0	0	0	0	0	0	0	0	0	0	0	82	18	. 0
	Poland	0	0	0	. 0	0	5	0	0	0	9	0	36	-50	0
	Younggwang	0	0	0	52	0	0	0	0	0	0	0	0	0	:48
		Brazil	Chile	Guerande	Haenam	Hokkaido	India	Jeung-Do	Kochi	Laizhou	Mongolia	Okinawa	Pakistan	Poland	Younggwang

Response

(c) Fused data model

	Brazil	100	0	0	0	0	0	0	0	0	0	0	0	0	0
	Chile	0	100	0	0	0	0	0	0	0	0	0	0	0	0
	Guerande	0	0	100	0	. 0	0	0	Ò	0	0	Ø	0	0	0
	Haenam	0	0	0	67	0	0	0	0	0	0	. 0	0	0	33
	Hokkaido	0	0	.0	0	100	0	0	.0	0	0	0	0	0	0
	India	0	-0	0	0	0	1.00	0	0	0	0	0	0	0	0
5	Jeung-Do	0	0	0	-0	0	0	100	0	0	0	0	0	0	0
Truth	Kochi	0	0	0	0	0	0	0	100	.0	0	0	0	0	0
	Laizhou	0	0	0	-0	0	0	0	:0	100	0	0	0	0	0
	Mongolia	-0	0	0	0	0	0	0	.0	0	100	0	0	0	0
	Okinawa	0	0	0	-0	0	0	0	.0	0	0	100	. 0	0	0
	Pakistan	0	0	0	0	0	0	0	0	0	0	0	100	-0	0
	Poland	0	0	0	0	0	0	0	0	0	0	- 5	0	-95	0
	Younggwang	0	0	0	0	0	0	0	0	0	0	0	0	0	100
		Brazil	ejje G	Guerande	Наепаш	Hokkaido	India	Jeung-Do	Kochi	Laizhou	Mongolia	Okinawa	Pakistan	Poland	Younggwang

Response

 $\begin{tabular}{ll} \textbf{Fig. 7.} Confusion matrices of the PLS-DA models based on LIBS (a), LA-ICP-MS (b), and their fused data (c). \end{tabular}$

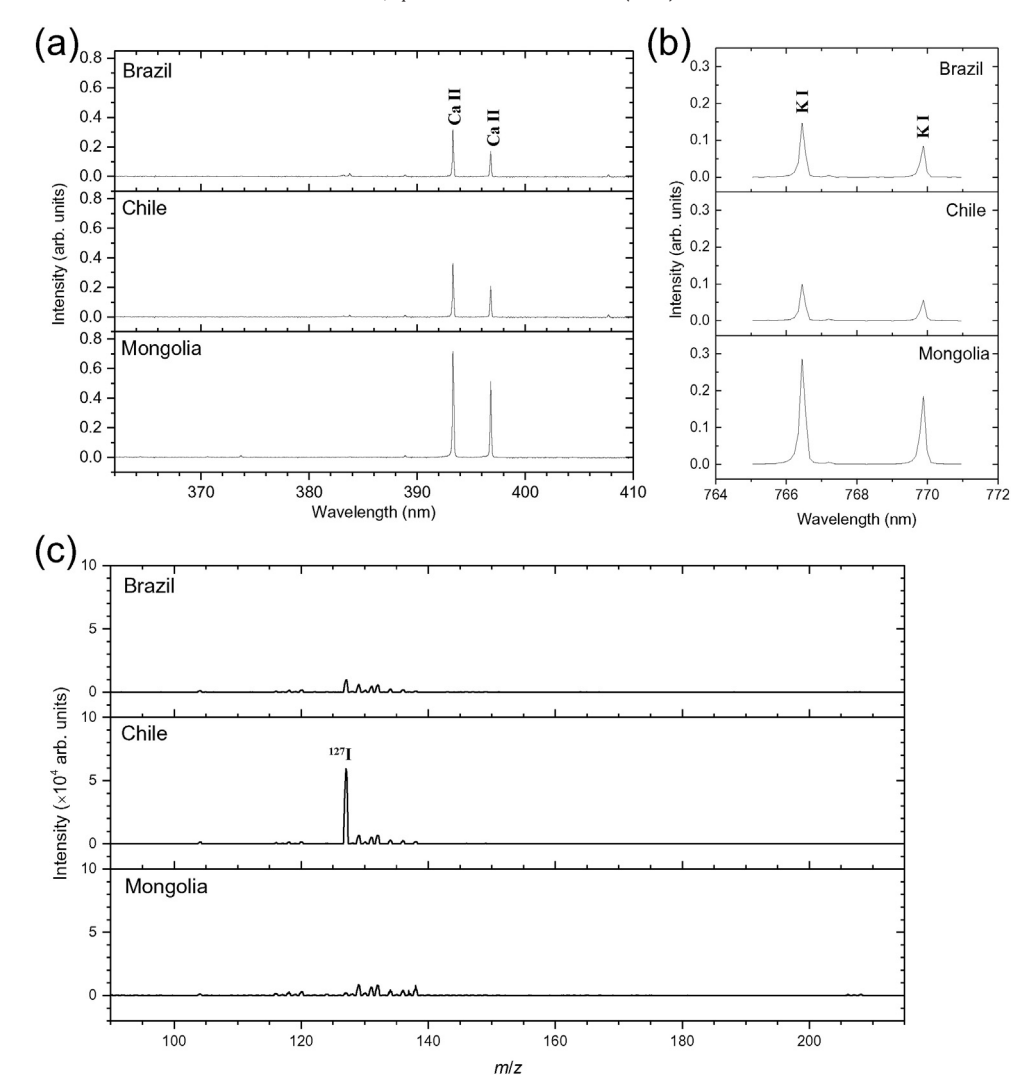


Fig. 8. LIBS spectra in the ultraviolet-visible (a) and near-infrared (b) regions and LA-ICP-MS spectra of the salts samples from Brazil, Chile, and Mongolia.

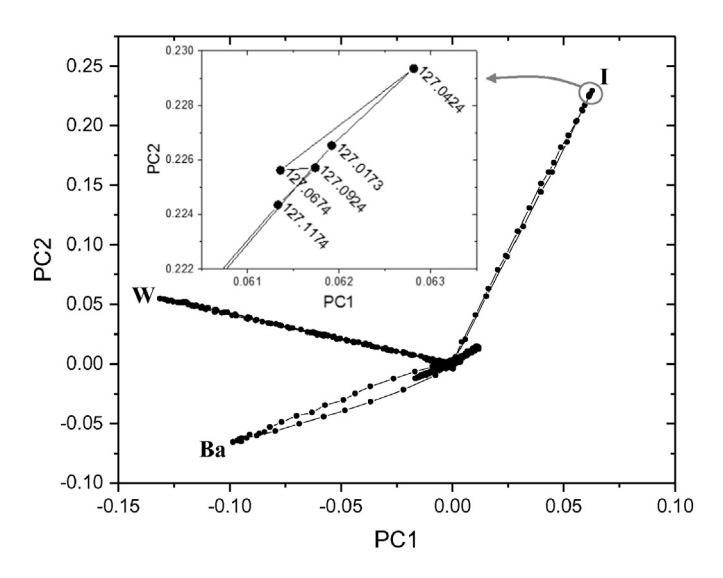


Fig. 9. Two-dimensional loading plot that shows the relationship between PC1 and PC2 extracted from the LA-ICP-MS spectra and also the relationship between the mass signal intensity at each m/z and the latent variables. The variables (data points in the LA-ICP-MS spectra) corresponding to I, W, and Ba isotopes are indicated. Also, the inset shows the expanded plot around the area of 127 I isotope mass signal with the corresponding m/z values.

wavelength region shows a similar confusion matrix to that based on the LIBS spectra in the selected wavelength (Fig. S1 in the Supplementary content); that the selected regions in LIBS spectra provided most of the discriminating power that can be extracted from the full spectra.

For all three models based on the different data sets (LIBS, LA-ICP-MS, and their fused data), inclusion of more PLS factors leads to higher CV correctness scores. However, the CV correctness tends to saturate since PLS factors later than around PC10 are not effective at discrimination compared to the major factors. For most cases with different numbers of PLS factors, the LIBS model shows the higher CV correctness scores than those of the LA-ICP-MS model. The maximum (or saturated) CV correctness score of the LIBS model is higher than that of the LA-ICP-MS model by ~20%. From these results, the LIBS spectra are found to be more effective in classifying the sample salts than the LA-ICP-MS spectra. However, the model based on the LIBS LA-ICP-MS fused data shows the highest CV correctness score and has more effective factors before the CV correctness score saturates. This result shows that the LA-ICP-MS spectra do provide discrimination power complementary to that of the LIBS spectra although the LA-ICP-MS model was not as effective as the LIBS model. The larger number of effective PLS factors in the model based on the fused data compared to those of the LIBS and LA-ICP-MS spectra is consistent with this result.

Fig. 7 shows the confusion matrices generated from the CV using LOO algorithm for the PLS-DA models using the LIBS (a), LA-ICP-MS

(b), and fused data (c). To avoid over-fitting the models, we chose the number of factors corresponding to a break from monotonically increasing the correctness scores for each model (9, 10, and 12 PLS factors for the LIBS, LA-ICP-MS, and fused data models, respectively). All correctness values in the confusion matrices are in %. The overall LLO CV correctness scores of the model based on the fused data is 97.4% and those of LIBS and LA-ICP-MS models are 87.2 and 68.8%, respectively. From the confusion matrix in Fig. 7a, the main cause deteriorating the performance of LIBS model is identified as the poor discrimination capability of the salt sample from Brazil, even with 9 PLS factors. This sample is misidentified as the salt from Chile with 100% probability in the LOO CV. In the LA-ICP-MS model with 10 PLS factors, the salt sample from Brazil is also mostly misidentified as the Mongolian rock salt sample with only 9% correctness score. However, the model based on the fused data shows 100% correctness score for identification of the salt sample from Brazil. This result clearly demonstrates that the combination of chemical information from LIBS and LA-ICP-MS improves the classification performance of these edible salts. Fig. 8 shows the LIBS (a and b) and LA-ICP-MS (c) spectra of the salt samples from Brazil, Chile, and Mongolia. In the LIBS spectra, the emission lines from Ca and K are stronger for the Mongolian rock salt sample than the salt samples from Brazil and Chile. On the other hand, the emission lines from Mg are stronger for the Brazilian and Chilean salts than the Mongolian salt (Fig. 8a and b). This feature distinguishes the Brazilian salt well from the Mongolian salts. However, similar features of LIBS spectra between the salt samples from Brazil and Chile make it difficult to distinguish the Brazilian salt from the Chilean salt. In the PC score plot based on the LA-ICP-MS data (Fig. 4b), the Brazil salt cluster was well separated from that of the Chile salt cluster along the axis between PC1 and PC2. The LA-ICP-MS spectrum of the Brazilian salt is significantly different from that of the Chilean salt, but not much different from that of the Mongolian rock salt (Fig. 8c). The two-dimensional loading plot in Fig. 9 shows the relationship between PC1 and PC2 extracted from the LA-ICP-MS spectra and also their relationship with the measured mass signal intensity at each m/z value. Thus, we can find the contribution of each data point in the LA-ICP-MS spectra to PC1 and PC2 in this plot. The data points corresponding to ¹²⁷I have positions in this plot that correspond to the direction indicated by the arrow in Fig. 4b. The inset shows the expanded plot around the position where the data points corresponding to ¹²⁷I are located with the numbers indicating the m/z values. This means that the salt sample from Chile shows a strong ¹²⁷I isotope mass signal (high concentration of I), and this distinguishes the Chilean salt from the others. The ¹²⁷I signal intensity is ~6 times stronger in the LA-ICP-MS spectrum of the Chile salt than that of the Brazil salt (see Fig. 2a).

About half of the LIBS spectra of the sea salt from Haenam resulted in misidentification as the sea salts from Hokkaido and Younggwang (Fig. 7a). With the aid of LA-ICP-MS spectra, the misidentification to the sea salt from Hokkaido could be corrected; the corresponding misidentification probability was decreased from 19% to 0% by data fusion (Fig. 7c). This can be attributed to the higher concentrations of Ba, W, and Pb in the salt from Haenam than those in the salt from Hokkaido (compare the Ba, W, and Pb mass peak intensities of the two salts shown in Fig. 2). However, the LOO CV performance of the fused data model is still deteriorated mainly by the misidentification of the salt from Haenam as the salt from Younggwang (Fig. 7c). This is easily understood by the fact that both LIBS and LA-ICP-MS models show significant misidentifications for the two salt samples. In fact, the saltpans, where the two sea salts were produced, are very closely located in the southwest coast of South Korea.

Our simultaneous LIBS and LA-ICP-MS experiments were performed in He gas for optimum performance of LA-ICP-MS analysis. Since the emission lines from laser-induced plasmas are generally stronger in air than in He, we checked the detectability of LIBS in air for the elements such as I, Ba, W, and Pb observed by LA-ICP-MS in He. As a result, only a very weak Ba line could be measured by LIBS in air. Details for the

differences in LIBS spectra obtained in air and He are discussed in the Supplementary content.

4. Conclusion

Simultaneous LIBS and LA-ICP-MS analysis was demonstrated for the classification of edible salt samples. LIBS and LA-ICP-MS were found to classify the sample salts in different ways. The two different data sets were fused to have similar contribution to the main features (not to be dominated by one part) with an appropriately selected weighting factor. The LIBS spectra provided a model with significantly higher LOO CV performance than that based on the LA-ICP-MS spectra of heavier elements ($m/z \ge 90$). The fusion of LIBS and LA-ICP-MS data provided the best performance than those of both LIBS and LA-ICP-MS models alone; the two elemental analyses data sets provide complementary information for salt classification. The fused data model gains most discrimination power from the LIBS spectra. Additionally, the chemical information about non-metals and trace heavy metals (I, Ba, W, and Pb) from the LA-ICP-MS spectra is effective in classifying some particular salt samples. The LIBS and LA-ICP-MS have strengths in analysis of different kinds of elements at different concentration levels. This enables the combination of LIBS and LA-ICP-MS to simultaneously provide more accurate chemical fingerprints for the classification of edible

Acknowledgment

This paper was supported by Research Funds of Mokpo National University in 2015, and a Grant 20130290 to the Solar Salt Research Center, Mokpo National University (MNU), from Ministry of Oceans and Fisheries of Korea. The research at the Lawrence Berkeley National Laboratory was supported by the Office of Basic Energy Sciences, Chemical Science Division of the U.S. Department of Energy under contract number DEAC02-05CH11231.

Appendix A. Supplementary data

Supplementary data to this article can be found online at http://dx.doi.org/10.1016/j.sab.2016.02.019.

References

- [1] M. O'Donnell, M.J. McQueen, H. Yan, A. Rosengren, A. Averzum, R. Iqbal, S. Gulec, R. Yusuf, G. Dagenais, S. Yusuf, Urinary sodium and potassium excretion, mortality, and cardiovascular events, N. Engl. J. Med. 371 (2014) 612–623.
- [2] M.J. Morris, E.S. Na, A.K. Johnson, Salt craving: the physiology of pathogenic sodium intake, Physiol. Behav. 94 (2008) 709–721.
- [3] M.H. Alderman, Salt, blood pressure and health: a cautionary tale, Int. J. Epidemiol. 31 (2002) 311–316.
- [4] F.J. He, G.A. MacGregor, Reducing population salt intake worldwide: from evidence to implementation, Prog. Cardiovasc. Dis. 52 (2010) 363–382.
- [5] C.M. Champagne, K.C. Lastor, Sodium intake: challenges for researchers attempting to assess consumption relative to health risks, J. Food Compos. Anal. 22S (2009) S19–S22.
- [6] E.I. Ekinci, K. Cheong, S. Clarke, R.J. MacIsaac, M.C. Thomas, G. Jerums, J.L. Moran, Dietary salt intake and mortality in patients with type 2 diabetes, Diabetes Care 34 (2011) 703–709.
- [7] Salt production method, http://www.saltinstitute.org/salt-101/production-industry/.
- [8] T.-C. Gao, J.-Y. Cho, L.-Y. Feng, S. Chanmuang, S.-Y. Park, C.-K. Auh, T.-K. Pai, K.-S. Ham, Mineral-rich solar sea salt generates less oxidative stress in rats than mineral-deficient salt, Food Sci. Biotechnol. 23 (2014) 951–956.
- [9] T. Kawasaki, K. Itoh, M. Kawasaki, Reduction in blood pressure with a sodiumreduced, potassium- and magnesium-enriched mineral salt in subjects with mild essential hypertension, Hypertens. Res. 21 (1998) 235–243.
- [10] E.S. Sarkkinen, M.J. Kastarinen, T.H. Niskanen, P.H. Karjalainen, T.M. Venäläinen, J.K. Udani, L.K. Niskanen, Feasibility and antihypertensive effect of replacing regular salt with mineral salt—rich in magnesium and potassium—in subjects with mildly elevated blood pressure, Nur. J. 10 (2011) 88.
- [11] P.E. Ray, S.I. Suga, X.H. Liu, R. Johnson, Chronic potassium depletion induces renal injury, salt sensitivity, and hypertension in young rats, Kidney Int. 59 (2001) 1850–1858.

- [12] A.C. Galvis-Sánchez, J.A. Lopes, I. Delgadillo, A.O.S.S. Rangel, Fourier transform near-infrared spectroscopy application for sea salt quality evaluation, J. Agric. Food Chem. 59 (2011) 11109–11116.
- [13] A. Günter, D. Knake, J. Schneider, H. Peters, Geochemistry of modern seawater and brines from salt pans: main components and bromine distribution, Contrib. Mineral. Petrol. 40 (1973) 1–24.
- [14] Y. Lee, K.-S. Ham, S.-H. Han, J. Yoo, S. Jeong, Revealing discriminating power of the elements in edible sea salts: line-intensity correlation analysis from laser-induced plasma emission spectra, Spectrochim. Acta Part B 101 (2014) 57–67.
- [15] M.M. Tan, S. Cui, J. Yoo, S.-H. Han, K.-S. Ham, S.-H. Nam, Y. Lee, Feasibility of laser-induced breakdown spectroscopy (LIBS) for classification of sea salts, Appl. Spectrosc 66 (2012) 262–271
- [16] M.A. Herrador, A.G. González, A.G. Asuero, Inorganic indicators of the origin of edible salts marketed in Spain from a chemometric approach, J. Food Prot. 61 (1998) 891–895
- [17] I. Silva, S.M. Rocha, M.A. Coimbra, Headspace solid phase microextraction and gas chromatography—quadrupole mass spectrometry methodology for analysis of volatile compounds of marine salt as potential origin biomarkers, Anal. Chim. Acta 635 (2009) 167–174.
- [18] D.W. Hahn, N. Omenetto, Laser-induced breakdown spectroscopy (LIBS), part II: review of instrumental and methodological approaches to material analysis and applications to different fields, Appl. Spectrosc. 66 (2012) 347–419.
- [19] N.S. Mokgalaka, J.L. Gardea-Torresdey, Laser Ablation Inductively Coupled Plasma Mass Spectrometry: principles and applications, Appl. Spectrosc. Rev. 41 (2006) 131–150.
- [20] R.E. Russo, X. Mao, J.J. Gonzalez, V. Zorba, J. Yoo, Laser ablation in analytical chemistry, Anal. Chem. 85 (2013) 6162–6177.
- [21] F.J. Fortes, J. Moros, P. Lucena, L.M. Cabalín, J.J. Laserna, Laser-induced breakdown spectroscopy, Anal. Chem. 85 (2013) 640–669.
- [22] E.H. Evans, J. Pisonero, C.M.M. Smith, R.N. Taylor, Atomic spectrometry update: review of advances in atomic spectrometry and related techniques, J. Anal. At. Spectrom. 30 (2015) 1017–1037.
- [23] J.S. Becker, State-of-the-art and progress in precise and accurate isotope ratio measurements by ICP-MS and LA-ICP-MS, J. Anal. At. Spectrom. 17 (2002) 1172–1185.
- [24] F. Vanhaecke, M. Resano, J. Koch, K. McIntosh, D. Günther, Femtosecond laser ablation-ICP-mass spectrometry analysis of a heavy metallic matrix: determination of platinum group metals and gold in lead fire-assay buttons as a case study, J. Anal. At. Spectrom. 25 (2010) 1259–1267.
- [25] X. Mao, A.A. Bol'shakov, I. Choi, C.P. McKay, D.L. Perry, O. Sorkhabi, R.E. Russo, Laser Ablation Molecular Isotopic Spectrometry: strontium and its isotopes, Spectrochim. Acta Part B 66 (2011) 767–775.
- [26] T. Trejos, A. Flores, J.R. Almirall, Micro-spectrochemical analysis of document paper and gel inks by laser ablation inductively coupled plasma mass spectrometry and

- laser induced breakdown spectroscopy, Spectrochim. Acta Part B 65 (2010) 884–895
- [27] M. Dong, D. Oropeza, J. Chirinos, J.J. González, J. Lu, X. Mao, R.E. Russo, Elemental analysis of coal by tandem laser induced breakdown spectroscopy and laser ablation inductively coupled plasma time of flight mass spectrometry, Spectrochim. Acta Part B 109 (2015) 44–50.
- [28] J.R. Chirinos, D.D. Oropeza, J.J. Gonzalez, H. Hou, M. Morey, V. Zorba, R.E. Russo, Simultaneous 3-dimensional elemental imaging with LIBS and LA-ICP-MS, J. Anal. At. Spectrom. 29 (2014) 1292–1298.
- [29] K. Subedi, T. Trejos, J. Almirall, Forensic analysis of printing inks using tandem Laser Induced Breakdown Spectroscopy and Laser Ablation Inductively Coupled Plasma Mass Spectrometry, Spectrochim, Acta Part B 103-104 (2015) 76–83.
- [30] C. Latkoczy, T. Ghislain, Simultaneous LIBS and LA-ICP-MS analysis of industrial samples. J. Anal. At. Spectrom. 29 (2014) 1292–1298.
- [31] M. Bonta, J.J. Gonzalez, C.D. Quarles Jr., R.E. Russo, B. Hegedus, A. Limbeck, Elemental mapping of biological samples by the combined use of LIBS and LA-ICP-MS, J. Anal. At. Spectrom. 31 (2016) 252–258.
- [32] G. Park, H. Yoo, Y. Gong, S. Cui, S.-H. Nam, K.-S. Ham, J. Yoo, S.-H. Han, Y. Lee, Feasibility of rapid classification of edible salts by a compact low-cost laser-induced breakdown spectroscopy device, Bull. Kor. Chem. Soc. 36 (2015) 189–197.
- [33] S.L. Drake, M.A. Drake, Comparison of salty taste and time intensity of sea and land salts from around the world, J. Sens. Stud. 26 (2011) 25–34.
- [34] M. Soylak, D.S.K. Peker, O. Turkoglu, Heavy metal contents of refined and unrefined table salts from Turkey, Egypt and Greece, Environ. Monit. Assess. 143 (2008) 267–272
- [35] H. Pourgheysari, M. Moazeni, A. Ebrahimi, Heavy metal content in edible salts in Isfahan and estimation of their daily intake via salt consumption, Int. J. Environ. Health Eng. 1 (2012) 41–45.
- [36] S.H. Tan, G. Horlick, Background spectral features in inductively coupled plasma/ mass spectrometry, Appl. Spectrosc. 40 (1986) 445–460.
- [37] N.M. Reed, R.O. Cairns, R.C. Hutton, Characterization of polyatomic ion interferences in inductively coupled plasma mass spectrometry using a high resolution mass spectrometer, J. Anal. At. Spectrom. 9 (1994) 881–896.
- [38] K.H. Esbensen, Multivariate Data Analysis—In Practice, 5th ed. CAMO Inc., 2004 349.
- 39] NIST Atomic Spectra Database, http://www.nist.gov/pml/data/asd.cfm.
- [40] N.B. Zorov, A.A. Gorbatenko, T.A. Labutin, A.M. Popov, A review of normalization techniques in analytical atomic spectrometry with laser sampling: from sample to multivariate correction, Spectrochim. Acta Part B 65 (2010) 642–657.
- 41] K.H. Esbensen, Multivariate Data Analysis—In Practice, 5th ed. CAMO Inc., 2004 163–164.